HHS Public Access

Author manuscript

Cell Rep. Author manuscript; available in PMC 2017 July 19.

Published in final edited form as:

Cell Rep. 2017 May 09; 19(6): 1257–1267. doi:10.1016/j.celrep.2017.04.048.

A Chimeric Egfr Protein Reporter Mouse Reveals Egfr Localization and Trafficking *in Vivo*

Yu-Ping Yang[1,2,11], **Haiting Ma**[1,2,11], **Alina Starchenko**[2,3], **Won Jae Huh**[2,4], **Wei Li**[1,2], **F. Edward Hickman**[5], **Qin Zhang**[1,2], **Jeffrey L. Franklin**[1,2,3,10], **Douglas P. Mortlock**[6], **Sabine Fuhrmann**[3,7], **Bruce D. Carter**[5], **Rebecca A. Ihrie**[3,8,9], and **Robert J. Coffey**[1,2,3,10,12,*]

[1]Department of Medicine, Vanderbilt University Medical Center

[2]Epithelial Biology Center, Vanderbilt University Medical Center

[3]Department of Cell and Developmental Biology, Vanderbilt University

[4]Department of Pathology, Microbiology and Immunology, Vanderbilt University Medical Center

[5]Department of Biochemistry, Vanderbilt University

[6]Department of Molecular Physiology and Biophysics, Vanderbilt University

[7]Department of Ophthalmology and Visual Sciences, Vanderbilt University Medical Center

[8]Department of Cancer Biology, Vanderbilt University

[9]Department of Neurological Surgery, Vanderbilt University Medical Center

[10]Department of Veterans Affairs Medical Center, Nashville, TN 37232

Summary

EGF receptor (EGFR) is a critical signaling node throughout life. However, it has not been possible to directly visualize endogenous Egfr in mice. Using CRISPR/Cas9 genome editing, we appended a fluorescent reporter to the C-terminus of the Egfr. Homozygous reporter mice appear normal and EGFR signaling is intact *in vitro* and *in vivo.* We detect distinct patterns of Egfr expression in progenitor and differentiated compartments in embryonic and adult mice. Systemic delivery of EGF or amphiregulin results in markedly different patterns of Egfr internalization and trafficking in hepatocytes. In the normal intestine, Egfr localizes to the crypt rather than villus compartment, expression is higher in adjacent epithelium than in intestinal tumors, and following colonic injury expression appears in distinct cell populations in the stroma. This reporter, under

[*]Correspondence: Robert J. Coffey, MD, Epithelial Biology Center, 10415 MRB IV, Vanderbilt University Medical Center, Nashville, TN 37232-0441, Phone: 615-343-6228; Fax: 615-343-1591, robert.coffey@vanderbilt.edu.

[11]These authors contributed equally

[12]Lead Contact

Author Contributions

Conceptualization, R.J.C. and Y.-P.Y.; Investigation, Y.-P.Y., A.S., W.J.H., W.L., Q.Z., E.H., R.A.I., S.F., B.D.C. and R.J.C.; Writing – Original Draft, Y.-P.Y., W.J.H., R.A.I., S.F. and R.J.C; Writing – Review & Editing, Y.-P.Y., J.L.F. and R.J.C; Resources, H.M. and D.P.M; Funding Acquisition, R.J.C.

control of its endogenous regulatory elements, enables *in vivo* monitoring of the dynamics of Egfr localization and trafficking in normal and disease states.

Graphical Abstract

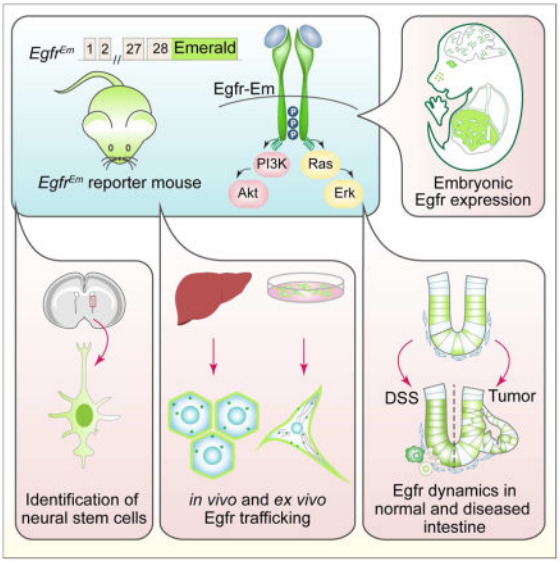

Keywords

Egfr; protein reporter; CRISPR/Cas9; amphiregulin; intracellular trafficking; neural stem cells; intestinal stem cells

Introduction

Over 50 years ago, Stanley Cohen discovered EGF and subsequently provided the initial biochemical characterization of its receptor, EGFR/ERBB1 (Carpenter and Cohen, 1976; Cohen, 1962). Since then, much has been learned, including the crystal structure of the EGFR ectodomain, kinase domains, and cytosolic tail (Lemmon et al., 2014; Schlessinger, 2014). EGFR is a glycosylated type 1 transmembrane protein with intrinsic tyrosine kinase activity that is triggered by ligand binding. Seven mammalian ligands bind to EGFR: four high affinity ligands (EGF, TGF-α [TGFA], HB-EGF [HBEGF] and β-cellulin [BTC]) and three low affinity ligands (amphiregulin [AREG], epiregulin [EREG] and epigen [EPGN]) (reviewed in Singh and Coffey, 2014). The ligands are produced as type 1 transmembrane precursors that can be cleaved by cell-surface proteases to produce mature soluble ligand. Ligand binding to EGFR results in homo- and hetero-dimerization of EGFR with other ERBB receptors (ERBB2–4), especially ERBB2. Ligand binding activates intrinsic tyrosine kinase activity, resulting in transphosphorylation of partnered receptors and initiation of a complex signal transduction cascade. There is accumulating evidence that the different ligands may confer quantitative and qualitative differing effects *in vitro* (Wilson et al., 2009), although this possibility has not been examined *in vivo*.

While EGFR is widely expressed, it is especially important in epithelial cell biology. Under normal physiological condition, it mediates a diverse range of biological functions, including cell growth, migration and differentiation (Schneider and Yarden, 2016). Genetic events leading to *EGFR* gain-of-function, either mutations or amplification, have been detected in individuals with multiple types of cancer including glioblastoma multiforme and lung cancer where such alterations have been validated as key drivers of these cancers (Schneider and Yarden, 2016). Furthermore, therapies targeting EGFR in epithelial malignancies by monoclonal antibodies against the EGFR ectodomain or EGFR tyrosine kinase inhibitors are deployed in colorectal, head and neck and lung cancer (Schneider and Yarden, 2016).

Despite these advances, there remain significant gaps in our knowledge. Much of what has been learned has relied on *in vitro* models, often using heterologous systems and applying non-physiological amounts of ligand. A major obstacle in studying the actions of Egfr in the mouse is the lack of robust and reliable antibodies for immunohistochemical detection of Egfr. To circumvent this impediment, we generated a knock-in protein reporter allele leading to production of a full-length Egfr protein fused at the C-terminus with a bright green fluorescent epitope tag, Emerald GFP (Em). This chimeric reporter allows direct visualization of mouse Egfr protein in the embryo and selected adult tissues. We show the value of this reporter in monitoring Egfr cellular localization and subcellular dynamics in normal and pathological conditions, as well for live cell imaging of the receptor in cells derived from these mice.

Results

Generation of *Egfr^{Em}* knock-in reporter mice

To create a reporter that allows visualization of Egfr protein and recapitulates the full spectrum of Egfr regulation and dynamics *in vivo*, we modified the endogenous *Egfr* locus by inserting an Em tag followed by a V5 tag into exon 28 of the *Egfr* gene in frame and just proximal to the stop codon (Figure 1A). This was done via CRISPR/Cas9-mediated genome editing in mouse zygotes (referred to as *Egfr^{Em}*; details in Supplemental Experimental Procedures), creating a locus that produces an Egfr chimeric protein C-terminally tagged with Em and V5. Individual germline-transmitted founder lines were established. Correct targeting was confirmed by sequencing the full-length cDNA expressed by the modified locus and detection of Egfr-Em fluorescence in frozen sections prepared from mouse tails (Figure S1D). All lines with confirmed targeting showed similar Egfr-Em staining in the tissues examined.

Intercrossing *Egfr$^{Em/+}$* mice led to production of *Egfr$^{Em/Em}$* animals, which were born at the expected Mendelian ratio (Table S1). Furthermore, *Egfr$^{Em/Em}$* mice are indistinguishable from their littermates (wild-type and *Egfr$^{Em/+}$*) at all developmental and postnatal stages, and are fertile in inbred C57BL/6 or outbred CD1 backgrounds. To further test the production of the Egfr-Em fusion protein, we examined its expression in several tissues of adult mice (brain, liver, intestinal crypts) by immunoblot analysis (Figure 1B, S1A–C). As expected, only tissues with an *Egfr^{Em}* allele(s) showed a slower migrating band (~210 kD) compared to wild-type Egfr (~180 kD) detected by anti-EGFR antibodies, with the size

difference corresponding to the size of EmGFP (~27kD). The ~210 kD band was detected with anti-GFP antibodies in tissue lysates prepared from mice expressing Egfr-Em (Figure 1B, S1A–C). There was no evidence of a cleaved Em protein separate from the Egfr-tagged chimera (Figure S1B), an event that would complicate interpretation of reporter expression. Based on these data, we conclude that mice with the knock-in allele produce an Egfr-Em fusion protein at equivalent levels as wild-type Egfr.

Normal signaling and localization of Egfr-Em chimeric protein

To assess whether EGFR signaling is intact in Egfr-Em reporter mice, we compared EGFR tyrosine phosphorylation and downstream Akt and Erk signaling at various times following the administration of recombinant mouse EGF (50 ng/ml) to primary adipose-derived stem cell (ASC) cultures generated from wild-type and $Egfr^{Em/Em}$ mice. There was the expected transient increase in pAkt and pErk1/2, whereas tyrosine phosphorylation of Egfr (pY1092) persisted over the 60-minute time course (Figure 1C,D). Comparable levels of total Egfr, as well as similar dynamics of pEgfr, pAkt and pErk1/2, were seen in the cultured ASCs derived from wild-type and $Egfr^{Em/Em}$ mice (Figure 1C,D). In separate experiments, we compared the half-life of Egfr in ASC cultures from both genotypes in the presence of cycloheximide, with and without EGF. There were no significant differences in the half-life of wild-type Egfr protein and the Egfr-Em fusion protein under these experimental conditions (Figure S1E–H). Taken together, these findings suggest that the Egfr-Em chimeric protein is fully functional and behaves similarly to the wild-type Egfr protein.

To further demonstrate how this system can be utilized, time-lapse movies were prepared following addition of Rhodamine-labeled EGF (50 ng/ml) to serum-starved ASC cultures derived from $Egfr^{Em/Em}$ mice (Movie S1). Cytoplasmic co-localization of EGF and Egfr-Em was clearly detected by 3 minutes after addition of EGF (static images in Figure 1F, F1–3). At later time points, the intracellular Egfr-Em signal became more evident likely due to clustering of Egfr-Em (Figure 1G; Movie S1). The EGF/Egfr-Em complexes traffic along F-actin (Figure 1E–G; Movie S1). In addition, membrane ruffling was observed following EGF administration (Movie S1), a cellular response that is largely small GTPase Rac1-dependent (Ridley et al., 1992). These data demonstrate the feasibility of using cells derived from these Egfr-Em reporter mice for high-resolution imaging to monitor the trafficking of endogenous Egfr.

Egfr-Em expression in developing embryos

In the mouse, EGFR signaling participates in strain-dependent critical developmental processes, as reflected in the wide variety of background-dependent phenotypes of *Egfr* mutants, including preimplantation lethality, late gestational lethality, and perinatal mortality (Strunk et al., 2004; Threadgill et al., 1995; Wieduwilt and Moasser, 2008). To examine Egfr-Em distribution during development, we chose to focus on embryonic day (E)14.5, a time at which many complex structures and organs develop. At this time, we visualized wholemount $Egfr^{Em/Em}$ embryos by direct fluorescence (Figure 2A). Egfr-Em was detected throughout wholemount embryos with enrichment in the future whisker placodes in the maxillary region (w in Figure 2A). Other structures with heightened Egfr-Em fluorescence include the otic placode (ot in Figure 2A), a small region of epidermis superficial to the

trigeminal ganglion (bracket in Figure 2A), the skeletal muscle of the limbs (dotted line in Figure 2A), and interzones of the presumptive phalangeal joints (arrows in Figure 2A).

Sagittal sectioning of whole embryos revealed the distribution of Egfr-Em fluorescence in detail (Figure 2B; higher resolution is shown in Figure S2). Overall, the pattern of Egfr-Em correlates with *Egfr* mRNA detection at this stage (Diez-Roux et al., 2011). Expression was found in other distinct structures, including throughout the epidermis, the inner root sheath of the whisker follicles, the liver, the choroid plexi within the ventricles of the brain, the vasculature within the brain, the endocardium and myocardium of the cardiac outflow tract, the arch of the aorta, and bronchus of lung epithelium (Figure 2C,D, S2C–L).

Of interest, in the ventricular zone (VZ) of the forebrain, Egfr-Em-expressing cells were scattered at the apical (ventricular) surface (Figure 2E,E′). These cells also expressed the transcription factor Pax6, which is typically expressed in radial glial stem cells, but not markers found in more differentiated cell types, such as Tbr2, which marks intermediate progenitor cells (Figure 2E′) (Englund et al., 2005). Thus, Egfr-Em is selectively expressed in the embryonic neural progenitor cells, consistent with previous results using antibodies against Egfr that are no longer available (Sun et al., 2005).

The Egfr-Em is also expressed in diverse extraocular tissues in the embryonic mouse eye (Figure 2F–F″). Coronal cryostat sections revealed Egfr-Em present in the periocular mesenchyme surrounding the optic cup, in the extraocular muscles, in mesenchymal cells giving rise to the hyaloid vasculature in the vitreous, in the corneal mesenchyme and epithelium, in the eyelid epithelium (palpebral epidermis), as well as the palpebral and bulbar conjunctiva (Figure 2F,F′). This labeling pattern is consistent with previous studies reporting endogenous *Egfr* mRNA expression and corresponds to roles of EGFR in migration and proliferation of periocular epithelia and mesenchyme (Lillien and Wancio, 1998; Reneker et al., 1995; Reneker et al., 2000; Xia and Kao, 2004). The paired-like homeodomain transcription factor Pitx2 is expressed in the periocular mesenchyme and extraocular muscles at this age in the mouse embryo (Gage et al., 2005), and Egfr-Em co-stained with Pitx2 in the periocular mesenchyme, corneal mesenchyme, presumptive hyaloid vasculature and extraocular muscles (Figure 2F,F′).

Collectively, these data show the value of this reporter line to study spatiotemporal patterning of the Egfr during mouse embryogenesis.

Egfr-Em uncovers neural stem and progenitor cell expression in adult brain

EGFR signaling has been implicated in regenerative events in the adult mouse brain (Gallo and Deneen, 2014). The neural stem cell niche of the ventricular-subventricular zone (V-SVZ) contains EGF-responsive cells, as demonstrated by the requirement for EGF in neurosphere-propagating conditions and by direct visualization of Egfr-expressing cells within the intact niche (Codega et al., 2014; Reynolds et al., 1992; Reynolds and Weiss, 1992). Intriguingly, supraphysiological stimulation via intraventricular infusion of EGF results in invasion of V-SVZ-derived cells into the surrounding parenchyma, reminiscent of brain tumor cells (Doetsch et al., 2002). We therefore mapped the expression pattern of Egfr-Em in this niche, with DCX as a marker for differentiated migratory cells. Using

wholemount *en face* preparations of the lateral face of the V-SVZ, we observed Egfr-Em expression on a dividing cell with a radial morphology (Figure 3A,B), likely an “activated” B1 cell. Additionally, we identified many Egfr-Em-positive, DCX-negative perivascular cells (Figure 3C). DCX-positive migratory cells were largely Egfr-Em negative (Figure 3D), consistent with published data suggesting that Egfr-expressing cells are predominantly transit-amplifying precursors and a limited number of stem (B1) cells, which have been activated to divide (Codega et al., 2014; Pastrana et al., 2009; Shen et al., 2008).

Activated stem and transit-amplifying progenitor cells from the V-SVZ can be cultured *ex vivo* and remain proliferative in the presence of bFGF and EGF; under these culture conditions, nearly all spheres are thought to be derived from Egfr-expressing cells (Codega et al., 2014; Pastrana et al., 2009). Upon mitogen withdrawal, these cultured cells differentiate into neurons, astrocytes, and oligodendrocytes, which are expected to be Egfr-negative. We therefore prepared bulk neurosphere cultures from perinatal (postnatal day 6) $Egfr^{Em/Em}$ mice and observed the expression of Egfr-Em at different time points before and after induction of differentiation by growth factor withdrawal (Figure 3E). As expected, most neural precursor cells cultured in the presence of EGF and bFGF expressed Egfr-Em (Figure 3E1). The number of Egfr-Em-positive cells declined over time after removal of growth factors, while the number of DCX-positive neuroblasts increased (Figure 3E2–4). DCX/Egfr-Em double-positive cells were rarely observed in these cultures. Collectively, these findings provide an entry point to interrogate the dynamics of Egfr localization and movement in an adult neural stem cell niche under normal and pathophysiological conditions.

Differential trafficking of Egfr-Em in hepatocytes following systemic administration of EGF or AREG

Although differential trafficking of Egfr by different ligands has been described *in vitro* (Chung et al., 2005; Roepstorff et al., 2009; Wilson et al., 2009), it has not been studied *in vivo*. Based on the knowledge that EGFR is highly expressed in liver and our ability to directly visualize Egfr-Em fluorescence in embryonic and adult liver (Figure 2B), we chose to monitor hepatic Egfr-Em after systemic delivery of two EGFR ligands (Figure 4). Following intraperitoneal (i.p.) injection of equimolar concentrations of EGF, a high-affinity ligand, and AREG, a low-affinity ligand, mice were sacrificed at various times and the livers were processed for Egfr-Em immunofluorescence. At baseline, Egfr-Em fluorescence was predominantly at the plasma membrane of hepatocytes (Figure 4A1,6). However, we observed markedly different patterns of Egfr-Em fluorescence following administration of the two ligands. As early as 5 minutes after EGF, there was less Egfr-Em at the plasma membrane and the appearance of punctate fluorescence in the cytoplasm (Figure 4A2). This pattern was more pronounced at 30 minutes (Figure 4A3), and at two hours there was a marked reduction in overall Egfr-Em fluorescence (Figure 4A4). At 24 hours, Egfr-Em returned to its baseline predominantly plasma membrane distribution (Figure 4A5). In marked contrast, following AREG, Egfr-Em fluorescence remained largely at the plasma membrane throughout the 24-hour time course (Figure 4A6–10), although some punctate cytosolic staining was observed at 30 minutes and 2 hours (Figure 4A8,9). We quantified the percent of Egfr-Em at the plasma membrane by analyzing its co-localization to that of a

plasma membrane marker, Na^+/K^+ ATPase (Figure 4B); at 30 minutes and 2 hours there was significantly less Egfr at the plasma membrane of hepatocytes following EGF compared to AREG treatment.

The high affinity ligand, EGF, triggered more robust tyrosine phosphorylation of Egfr compared to the low affinity ligand, AREG, as determined by immunoblotting of liver extracts; however, similar activation of downstream Erk and Akt was found with both ligands (Figure S4A). We did observe an interesting early difference in the pattern of pErk1/2 immunofluorescence in hepatocytes following i.p. injection of the two ligands (Figure 4C). At baseline, little, if any, pErk1/2 staining was detected (Figure 4C1,3). Five minutes after EGF, nuclear pErk1/2 was evenly distributed throughout the hepatocytes (Figure 4C2). In contrast, there was a gradient of nuclear staining of hepatocytes from the portal tract to the central vein five minutes after AREG (Figure 4C4). Thirty minutes after EGF or AREG, there was no difference in pErk1/2 staining (Figure S4B,C).

To assess which intracellular compartments Egfr-Em was traversing following delivery of these two ligands, we co-stained with intracellular compartment-selective markers (Figure 4D,E). As expected, at 30 minutes after EGF, there was considerable Egfr-Em co-localization with the early endosome marker Eea1 that was much reduced at 2 hours (Figure 4D1,2). At 30 minutes, there was occasional co-localization of the Egfr-Em with the lysosomal marker, Lamp1 (Figure 4E1); this co-localization was more apparent at 2 hours and this coincided with the marked reduction in Egfr-Em (Figure 4E2). In contrast, after AREG, there was considerable co-localization of Egfr-Em and Eea1 at 30 minutes and 2 hours (Figure 4D3,4); co-localization of Egfr-Em and Lamp1 was much less than after EGF (Figure 4E3,4). Thus, Egfr-Em is endocytosed and then degraded in a lysosomal compartment after EGF treatment, whereas following AREG treatment it appears to be endocytosed, but there is much less lysosomal degradation. Future studies will be needed to more precisely determine how much Egfr-Em is endocytosed and which recycling compartment it utilizes following AREG delivery.

Dynamic Egfr-Em expression in the epithelium and stroma of the small intestine

We next examined distribution of Egfr-Em in tissue sections of the small intestine of *Egfr*$^{Em/Em}$ adult mice (Figure 5). Within the epithelium, staining was chiefly in the crypt compared to the villus compartment (Figure 5A); this was confirmed by immunoblotting of crypt and villus fractions (Figure S1C). Although every crypt showed Egfr-Em expression, ~30% of crypts showed much higher expression (arrows in Figure 5A, S5A). As shown at higher power in Figure 5B, staining in the duodenum was more prominent in the crypt-based columnar cells than neighboring Paneth cells marked by c-Kit. In addition, staining appeared more intense in the transit-amplifying compartment than at the crypt base (Figure 5B,C). Both membranous and cytosolic Egfr staining were observed, whereas pEgfr (pY1092) appeared confined to the plasma membrane (asterisks in Figure 5C). To further elucidate if this pattern is consistent with the activation of downstream EGFR signaling in the intestinal crypts, we examined the expression pattern of pErk1/2 by immunostaining. pErk1/2 is highly enriched in a subset of stem and progenitor cells within the transit-amplifying zone of intestinal crypts (Figure 5D), which largely overlap with the expression domain of Egfr-Em

(Figure 5D′,D″). Therefore, Egfr-Em, pEgfr and pErk1/2 show similar and overlapping expression patterns within the normal small intestinal crypts. In the colon, membranous Egfr-Em was detected throughout the length of the crypts (Figure S5D–F).

Egfr-Em was also detected in non-epithelial cells. Staining was enriched throughout the outer longitudinal muscle layer compared to the inner circular muscle layer (brackets in Figure 5A,E; Figure S5C–E). We recently identified that the pan-ErbB inhibitor, Lrig1, marks intestinal stem/progenitor cells (Powell et al., 2012) and a subset of interstitial cells of Cajal (ICC), the intestinal pacemaker (Kondo et al., 2015). These ICC cells do not express Egfr-Em, but are surrounded by Egfr-Em^{+} cells that are fibroblast-like cells expressing PDGFRα (Figure 5E″, S5G) (Iino et al., 2009). In the overlying epithelium, however, Lrig1 and Egfr-Em are co-expressed (Figure 5E′), suggesting the context-dependent expression pattern of Egfr and Lrig1.

Colonic organoids were established from heterozygous Egfr-Em mice (Figure 5F). Under basal growth conditions, Egfr-Em staining was detected in the cytosol of a subset of cells (asterisks in Figure 5F1). Upon removal of serum and growth factors for 48 hours, much reduced membranous staining was observed (Figure 5F2). After 30 minutes of exposure to EGF, numerous cells exhibited punctate cytosolic staining (arrows in Figure 5F3). Thus, these colonic organoids recapitulate the *in vivo* pattern of Egfr-Em in intestinal crypts, respond to exogenous stimulation, and, like the ASC cultures (Figure 1E–G), show the feasibility of monitoring EGFR dynamics *ex vivo*.

Alterations of Egfr expression in the gut under pathological conditions

Since disruption of EGFR signaling has been implicated in many pathological conditions in the gastrointestinal tract, we next explored the utility of using this reporter to monitor Egfr in the setting of intestinal neoplasia and colonic inflammation. We previously reported that 50 days after tamoxifen-induced elimination of one *Apc* allele in $Lrig1^{CreER/+};Apc^{fl/+}$ mice tumors are detected in small intestine and colon with the expected stochastic loss of the second *Apc* allele (Powell et al., 2014; Powell et al., 2012). We introduced $Egfr^{Em}$ reporter into this background, and, as expected, tumors were found in the small intestine of these $Lrig1^{CreER/+};Apc^{fl/+};Egfr^{Em/+}$ mice 50 days after tamoxifen induction. There was heterogeneous expression of Egfr-Em and pEgfr in the tumors with pEgfr often more intense than Egfr-Em (Figure 6A–D, S6A,B). We consistently detected strong Egfr-Em in a rim of grossly normal epithelium surrounding the tumors (Figure 6A and S6A,B).

To further examine the heterogeneity of Egfr-Em and pEgfr expression in the tumor, we compared the proportion of pEgfr and Egfr-Em co-expression relative to that of Egfr-Em in the tumor and normal crypts. Whereas the normal crypts showed a ~76% of correlation (n=68), only a ~55% of correlation was found within adenomas (n=21; Figure S6C). Of interest, high Lrig1 expression was often found in a subset of Egfr-Em-expressing tumor cells, and these cells often expressed lower Egfr-Em and high cytoplasmic β-catenin immunoreactivity (i.e. Lrig1^{HI}Egfr-Em^{LO}β-catenin^{HI}; arrows in Figure 6D1–3) when compared to the neighboring cells (Lrig1^{LO}Egfr-Em^{HI}β-catenin^{LO}; asterisks in Figure 6D1–3; S6D,E). The differences in Lrig1 and Egfr-Em expression in normal crypts and tumors

(Figure 5D versus 6D) suggest distinct regulatory mechanisms for Lrig1 and Egfr in these tissues.

We next investigated Egfr-Em expression in the colon following dextran sodium sulfate (DSS)-induced damage and inflammation (Perse and Cerar, 2012). Recent studies have shown that Egfr activation in immune cells in the gut promotes tissue restoration following injury (Dube et al., 2012; Hardbower et al., 2016; Monticelli et al., 2015). Of interest, Areg expression in group 2 innate lymphoid (ILC2) cells within the gut stroma has been implicated in these reparative events (Monticelli et al., 2015). We induced colitis in *Egfr*$^{Em/+}$ *mice* by exposure to 2.5% DSS in the drinking water and examined Egfr-Em expression during acute damage and subsequent repair. After 7 days of DSS, there was colonic epithelial disruption, loss of crypts, and immune cell infiltration (Figure 6F). Near full recovery of the mucosa was found 7 days after DSS withdrawal (Figure S6F3).

In control mice, Areg was enriched at the luminal surface of the colonic epithelium (Figure 6E) as previously reported (Johnson et al., 1992). Areg^{+} cells were also detected in the lamina propria expressing low Egfr-Em (arrows in Figure 6E). After 7 days of exposure to DSS, Egfr-Em was upregulated in the surviving epithelium (Figure 6F), and an increased number of F4/80^{+}Em^{HI}Areg^{+} macrophages infiltrated into the mucosa (arrows in Figure 6F1–4). Other non-macrophage Egfr-Em^{HI}Areg^{+} immune cells were also distributed in the damaged mucosa and submucosal layer (Figure 6F). We did not see significant numbers of CD4^{+} or CD8a^{+} T cells expressing Egfr-Em in control or DSS-treated mice (Figure S6G,H). These events are transient since 7 days after DSS withdrawal Areg and Egfr expression and localization return to normal (Figure S6F3). We speculate that in the setting of acute inflammation infiltration of Areg-expressing immune cells and heightened Egfr-Em in the stroma and epithelium can lead to activation of EGFR signaling in both compartments. Further studies will be needed to delineate the consequences of EGFR activation in the different cell types that express Egfr-Em.

Thus, we present two pathological conditions - intestinal neoplasia and colonic damage - in which there are dynamic and unexpected patterns of Egfr protein localization in both epithelial and stromal cell types. These examples set the stage for more mechanistic studies underlying these observations, as well as monitoring Egfr localization and dynamics following other perturbations.

Discussion

Since robust and reliable antibodies for the immunohistochemical detection of Egfr in the mouse are lacking, we set out to generate an *Egfr* reporter mouse to better monitor Egfr protein *in vivo* using an epitope-tagged chimeric Egfr protein. We reasoned that such a reporter would give information beyond existing *Egfr* transcriptional reporters (Sibilia and Wagner, 1995) by providing a readout of the dynamics of Egfr protein localization and trafficking. This was achieved by appending epitope tags to the C-terminus of the Egfr protein within the endogenous *Egfr* locus by CRISPR/Cas9 genome editing. Emerald was selected as a tag since it is brighter and less likely to dimerize than EGFP (Day and Davidson, 2009) and a V5 tag was added to facilitate immunoprecipitation experiments.

One obvious concern was that the EGFP and V5 epitope tags would interfere with the function of Egfr. However, this did not appear to be the case. Homozygous *Egfr*^{Em} mice did not exhibit any detectable abnormality in either C57/BL6 inbred or CD1 outbred backgrounds, and mice were born at the expected Mendelian ratio (Table S1). The normality of *Egfr*^{Em} mice in other genetic backgrounds requires further investigation. Heterozygous and homozygous Egfr-Em mice were grossly normal in size and behavior. Egfr-Em localized to the basolateral surface of polarized epithelial cells (e.g. Figure 2,5). At the biochemical level, both EGF-initiated signaling and receptor half-life were qualitatively similar in ASC cells derived from Egfr-Em homozygous and wild-type mice (Figure 1C,D). Furthermore, no low molecular weight cleaved Emerald protein was detected from immunoblot analysis of multiple tissues from *Egfr*^{Em} mice (Figure S1B). Thus, based on multiple lines of evidence, we conclude that the Egfr-Em mouse faithfully recapitulates the regulation and function of endogenous Egfr.

The first biological effect noted for EGF was described by Stanley Cohen (Cohen, 1962). Upon subcutaneous injection of protein extracts isolated from submaxillary glands (later shown to be EGF) into newborn mice, he observed precocious eyelid opening at postnatal day 7 rather than day 12–14. Subsequent studies delineated roles for EGFR signaling in eyelid closure, particularly in regulating the migration and cytoskeletal dynamics of keratinocytes in the eyelid epithelium during embryonic development (Xia and Kao, 2004). The strong Egfr-Em expression we detected in the eyelid epithelium (Figure 2F) is in agreement with these observations. Egfr-Em expression in periocular mesenchyme, the corneal mesenchyme and the corneal epithelium (Figure 2F′) also corresponds to previous known TGFα-EGFR signaling activities in these structures. In this setting, TGFα most likely acts as a chemoattractant for migrating mesenchymal cells expressing Egfr (Grant et al., 1992; Mann et al., 1993; Reneker et al., 1995; Zieske et al., 2000).

This Egfr-Em reporter mouse will be a useful tool to better understand EGFR-related events in both the developing and adult mouse brain. Neural stem cells contribute to the development and ongoing homeostasis of the brain and potentially regeneration after damage, as well as having an important role in specific types of learning and memory (Bond et al., 2015). Activated neural stem cells in the V-SVZ (i.e. aB1 cells) and their transit-amplifying progeny are identified in part by their ability to respond to EGF and to generate neurospheres in EGF-enriched medium. To date, the majority of prospective enrichment strategies for isolating these cells have relied on acute administration of fluorescently-labeled EGF.

Our results showed that Egfr-Em labels cell with radial morphology, ventricular contact, and cell bodies basal to ependymal “pinwheels” (Figure 3, S3), features which are typical of aB1 cells (Mirzadeh et al., 2008; Shen et al., 2008; Tavazoie et al., 2008). Further, Egfr-Em^{+}DCX^{-} perivascular cells that lacked a radial morphology had the expected pattern of distribution for C cells. The *Egfr*^{Em} mouse should prove valuable for further analyzing the complex cellular niche of the V-SVZ germinal zone and prospectively isolating Egfr-Em^{+} cells without the use of exogenous ligand, as well as monitoring the behavior of Egfr-expressing neural stem cells in response to manipulation of the niche *in vivo*.

Early on, Stanley Cohen noted that EGFR levels were high in mouse liver (Cohen et al., 1982; Okeefe et al., 1974). This led him to conduct a series of experiments in which he injected EGF i.p. and he identified a number of biological effects in livers that were harvested shortly thereafter (Donaldson and Cohen, 1992; Ruffjamison et al., 1993a; Ruffjamison et al., 1993b; Ruffjamison et al., 1994). This prompted us to examine the trafficking of Egfr-Em in hepatocytes after systemic administration of EGF or AREG. Earlier studies investigated Egfr trafficking *in vivo* in rat liver upon EGF treatment, mostly using radio-labeled EGF and/or subcellular organelle fractionation (Chabot et al., 1986; Lai et al., 1989). Our results show that Egfr trafficking in hepatocytes differs markedly after systemic administration of equimolar concentrations of EGF or AREG that result in equivalent activation of EGFR downstream signaling in the liver (Figure S4). After EGF treatment, Egfr-Em is rapidly internalized and transits from early endosomes at 30 minutes to lysosomes at two hours, leading to diminished Egfr-Em at the plasma membrane and in the cytosol. In contrast, much less Egfr-Em is internalized after AREG treatment, and the small amount internalized is in early endosomes and rarely is found in lysosomes. These findings are consistent with previously reported *in vitro* data (Roepstorff et al., 2009) and confirm that EGFR trafficking can be studied *in vivo* using this Egfr-Em reporter mouse model.

An intriguing finding in these liver studies was the different pattern of nuclear pErk1/2 distribution in hepatocytes five minutes after systemic delivery of EGF and AREG. Upon i.p. injection, the ligands are rapidly taken by the vasculature and first delivered to the liver via the portal vein whereupon they diffuse through the sinusoids to the central vein of each liver lobule. We speculate that Erk1/2 in hepatocytes near the portal tracts are activated earlier than those near the central veins because of the direction of blood flow in the liver. The difference between EGF and AREG might be due to the difference in affinity and/or the heparin binding property of AREG. However, the possibility of intrinsic difference between hepatocytes near the portal vein and those near the central vein cannot be excluded. It will be interesting to treat EGF or AREG in liver-specific Apc knock-out mice and DKK1 over-expressing mice in which hepatic zonation is disturbed (Benhamouche et al., 2006). These findings underscore the value of this reporter mouse in monitoring Egfr dynamics *in vivo* after various perturbations.

The ability to visualize Egfr protein in this reporter mouse afforded us the opportunity to examine its location in the gut. We found that Egfr-Em is largely restricted to the crypt base of the small intestinal epithelium (Figure 5A,B). In this compartment, we see evidence of active Egfr and downstream signaling as determined by pEgfr and pErk1/2 (Figure 5C,D). Paneth cells produce EGF and TGFα (Sato et al., 2011), so it is likely that these ligands bind locally to and activate Egfr-expressing crypt cells. We also examined the relationship between Egfr-Em and its negative regulator, Lrig1 (reviewed in Wang, 2013). In the normal crypt compartment, there is overlapping expression of Egfr and Lrig1. In a subset of ICCs that express Lrig1, Egfr-Em is absent, leading us to speculate that Lrig1 is subserving its role as an Egfr negative regulator in these cells.

We observed heterogeneous Egfr-Em expression and altered regulation of Egfr in adenomas. In more dysplastic regions with high cytoplasmic/nuclear β-catenin, Lrig1 and Egfr-Em are

reversely correlated, whereas in less dysplastic regions Lrig1 and Egfr-Em are co-expressed, reminiscent of normal crypts (Figure 6). More dysplastic parts of the tumor also appear to have reduced co-expression of pEgfr and Egfr-Em (Figure 6B, S6C) that may indicate higher turnover and activation rates of Egfr within these domains. The enhanced expression of Egfr-Em in the stroma in the DSS-induced colitis model highlights the complexity of Egfr regulation (Figure 6F) and suggests that EGFR-targeted therapies may have direct effects on stromal immune cells. The *Egfr*^{Em} mouse model makes detailed longitudinal studies of Egfr localization and regulation under various conditions and disease models possible.

In summary, we established and validated an *Egfr*^{Em} protein reporter *in vivo* that faithfully recapitulates the endogenous Egfr expression at single-cell resolution. We propose that this mouse will be a valuable tool for studying EGFR signaling and receptor trafficking *in vivo*.

Experimental Procedures

Further details and an outline of resources used in this work can be found in Supplemental Experimental Procedures.

Mice

All experiments with mice were performed under protocols approved by the Vanderbilt University Medical Center Institutional Animal Care and Use Committee. For further details, see Supplemental Experimental Procedures. All mice used were within 6 month of age and no gender difference was found.

Statistical Methods

For densitometric quantification in cycloheximide chase assay, as well as for morphometric analysis of Egfr expression, quantifications were performed using ImageJ. Statistical significance was determined using a Student’s T-test for each analysis. The graphs represent means ± S.E.M. For further details, see Supplemental Experimental Procedures.

Supplementary Material

Refer to Web version on PubMed Central for supplementary material.

Acknowledgments

We thank G. Carpenter for critical reading of our manuscript, and the Coffey lab members for helpful discussions. This work was supported by NIH [CA46413, CA151566, CA163563, CA174377 and P50 95103 to R.J.C., EY024373 and P30-EY008126 to S.F., NS096238 to R.A.I]. It was also supported by an Unrestricted Grant from Research to Prevent Blindness, Inc. to S.F., DOD/TSCRP Idea Development Award TS150037 and two Discovery Grants from the Vanderbilt-Ingram Cancer Center to R.A.I. We acknowledge the Vanderbilt Transgenic Mouse/ES Cell Shared Resource, which is supported in part by the Vanderbilt-Ingram Cancer Center.

References

Benhamouche S, Decaens T, Godard C, Chambrey R, Rickman DS, Moinard C, Vasseur-Cognet M, Kuo CJ, Kahn A, Perret C, et al. Apc tumor suppressor gene is the “zonation-keeper” of mouse liver. Dev Cell. 2006; 10:759–770. [PubMed: 16740478]

Bond AM, Ming GL, Song HJ. Adult Mammalian Neural Stem Cells and Neurogenesis: Five Decades Later. Cell stem cell. 2015; 17:385–395. [PubMed: 26431181]

Carpenter G, Cohen S. 125I-labeled human epidermal growth factor. Binding, internalization, and degradation in human fibroblasts. The Journal of cell biology. 1976; 71:159–171. [PubMed: 977646]

Chabot JG, Walker P, Pelletier G. Distribution of Epidermal Growth-Factor Binding-Sites in the Adult-Rat Liver. Am J Physiol. 1986; 250:G760–G764. [PubMed: 3013022]

Chung E, Graves-Deal R, Franklin JL, Coffey RJ. Differential effects of amphiregulin and TGF-alpha on the morphology of MDCK cells. Experimental cell research. 2005; 309:149–160. [PubMed: 15979068]

Codega P, Silva-Vargas V, Paul A, Maldonado-Soto AR, Deleo AM, Pastrana E, Doetsch F. Prospective identification and purification of quiescent adult neural stem cells from their in vivo niche. Neuron. 2014; 82:545–559. [PubMed: 24811379]

Cohen S. Isolation of a mouse submaxillary gland protein accelerating incisor eruption and eyelid opening in the new-born animal. The Journal of biological chemistry. 1962; 237:1555–1562. [PubMed: 13880319]

Cohen S, Fava RA, Sawyer ST. Purification and Characterization of Epidermal Growth-Factor Receptor Protein-Kinase from Normal Mouse-Liver. P Natl Acad Sci-Biol. 1982; 79:6237–6241.

Day RN, Davidson MW. The fluorescent protein palette: tools for cellular imaging. Chemical Society reviews. 2009; 38:2887–2921. [PubMed: 19771335]

Diez-Roux G, Banfi S, Sultan M, Geffers L, Anand S, Rozado D, Magen A, Canidio E, Pagani M, Peluso I, et al. A high-resolution anatomical atlas of the transcriptome in the mouse embryo. PLoS biology. 2011; 9:e1000582. [PubMed: 21267068]

Doetsch F, Petreanu L, Caille I, Garcia-Verdugo JM, Alvarez-Buylla A. EGF converts transit-amplifying neurogenic precursors in the adult brain into multipotent stem cells. Neuron. 2002; 36:1021–1034. [PubMed: 12495619]

Donaldson RW, Cohen S. Epidermal Growth-Factor Stimulates Tyrosine Phosphorylation in the Neonatal Mouse - Association of a M(R) 55,000 Substrate with the Receptor. Proceedings of the National Academy of Sciences of the United States of America. 1992; 89:8477–8481. [PubMed: 1382290]

Dube PE, Yan F, Punit S, Girish N, McElroy SJ, Washington MK, Polk DB. Epidermal growth factor receptor inhibits colitis-associated cancer in mice. The Journal of clinical investigation. 2012; 122:2780–2792. [PubMed: 22772467]

Englund C, Fink A, Lau C, Pham D, Daza RA, Bulfone A, Kowalczyk T, Hevner RF. Pax6, Tbr2, and Tbr1 are expressed sequentially by radial glia, intermediate progenitor cells, and postmitotic neurons in developing neocortex. The Journal of neuroscience: the official journal of the Society for Neuroscience. 2005; 25:247–251. [PubMed: 15634788]

Gage PJ, Rhoades W, Prucka SK, Hjalt T. Fate maps of neural crest and mesoderm in the mammalian eye. Investigative ophthalmology & visual science. 2005; 46:4200–4208. [PubMed: 16249499]

Gallo V, Deneen B. Glial development: the crossroads of regeneration and repair in the CNS. Neuron. 2014; 83:283–308. [PubMed: 25033178]

Grant MB, Khaw PT, Schultz GS, Adams JL, Shimizu RW. Effects of epidermal growth factor, fibroblast growth factor, and transforming growth factor-beta on corneal cell chemotaxis. Investigative ophthalmology & visual science. 1992; 33:3292–3301. [PubMed: 1428704]

Hardbower DM, Singh K, Asim M, Verriere TG, Olivares-Villagomez D, Barry DP, Allaman MM, Washington MK, Peek RM Jr, Piazuelo MB, et al. EGFR regulates macrophage activation and function in bacterial infection. The Journal of clinical investigation. 2016

Iino S, Horiguchi K, Horiguchi S, Nojyo Y. c-Kit-negative fibroblast-like cells express platelet-derived growth factor receptor alpha in the murine gastrointestinal musculature. Histochem Cell Biol. 2009; 131:691–702. [PubMed: 19280210]

Johnson GR, Saeki T, Gordon AW, Shoyab M, Salomon DS, Stromberg K. Autocrine action of amphiregulin in a colon carcinoma cell line and immunocytochemical localization of amphiregulin in human colon. The Journal of cell biology. 1992; 118:741–751. [PubMed: 1639855]

Kondo J, Powell AE, Wang Y, Musser MA, Southard-Smith EM, Franklin JL, Coffey RJ. LRIG1 Regulates Ontogeny of Smooth Muscle-Derived Subsets of Interstitial Cells of Cajal in Mice. Gastroenterology. 2015; 149:407–419. e408. [PubMed: 25921371]

Lai WH, Cameron PH, Wada I, Doherty JJ, Kay DG, Posner BI, Bergeron JJM. Ligand-Mediated Internalization, Recycling, and down-Regulation of the Epidermal Growth-Factor Receptor Invivo. Journal of Cell Biology. 1989; 109:2741–2749. [PubMed: 2592403]

Lemmon MA, Schlessinger J, Ferguson KM. The EGFR family: not so prototypical receptor tyrosine kinases. Cold Spring Harbor perspectives in biology. 2014; 6:a020768. [PubMed: 24691965]

Lillien L, Wancio D. Changes in Epidermal Growth Factor Receptor Expression and Competence to Generate Glia Regulate Timing and Choice of Differentiation in the Retina. Molecular and cellular neurosciences. 1998; 10:296–308.

Mann GB, Fowler KJ, Gabriel A, Nice EC, Williams RL, Dunn AR. Mice with a null mutation of the TGF alpha gene have abnormal skin architecture, wavy hair, and curly whiskers and often develop corneal inflammation. Cell. 1993; 73:249–261. [PubMed: 8477444]

Mirzadeh Z, Merkle FT, Soriano-Navarro M, Garcia-Verdugo JM, Alvarez-Buylla A. Neural stem cells confer unique pinwheel architecture to the ventricular surface in neurogenic regions of the adult brain. Cell stem cell. 2008; 3:265–278. [PubMed: 18786414]

Monticelli LA, Osborne LC, Noti M, Tran SV, Zaiss DM, Artis D. IL-33 promotes an innate immune pathway of intestinal tissue protection dependent on amphiregulin-EGFR interactions. Proceedings of the National Academy of Sciences of the United States of America. 2015; 112:10762–10767. [PubMed: 26243875]

Okeefe E, Hollenbe Md, Cuatreca P. Epidermal Growth-Factor - Characteristics of Specific Binding in Membranes from Liver, Placenta, and Other Target Tissues. Arch Biochem Biophys. 1974; 164:518–526. [PubMed: 4376663]

Pastrana E, Cheng LC, Doetsch F. Simultaneous prospective purification of adult subventricular zone neural stem cells and their progeny. Proceedings of the National Academy of Sciences of the United States of America. 2009; 106:6387–6392. [PubMed: 19332781]

Perse M, Cerar A. Dextran sodium sulphate colitis mouse model: traps and tricks. Journal of biomedicine & biotechnology. 2012; 2012:718617. [PubMed: 22665990]

Powell AE, Vlacich G, Zhao ZY, McKinley ET, Washington MK, Manning HC, Coffey RJ. Inducible loss of one Apc allele in Lrig1-expressing progenitor cells results in multiple distal colonic tumors with features of familial adenomatous polyposis. American journal of physiology Gastrointestinal and liver physiology. 2014; 307:G16–23. [PubMed: 24833705]

Powell AE, Wang Y, Li Y, Poulin EJ, Means AL, Washington MK, Higginbotham JN, Juchheim A, Prasad N, Levy SE, et al. The pan-ErbB negative regulator Lrig1 is an intestinal stem cell marker that functions as a tumor suppressor. Cell. 2012; 149:146–158. [PubMed: 22464327]

Reneker LW, Silversides DW, Patel K, Overbeek PA. TGF alpha can act as a chemoattractant to perioptic mesenchymal cells in developing mouse eyes. Development. 1995; 121:1669–1680. [PubMed: 7600984]

Reneker LW, Silversides DW, Xu L, Overbeek PA. Formation of corneal endothelium is essential for anterior segment development - a transgenic mouse model of anterior segment dysgenesis. Development. 2000; 127:533–542. [PubMed: 10631174]

Reynolds BA, Tetzlaff W, Weiss S. A multipotent EGF-responsive striatal embryonic progenitor cell produces neurons and astrocytes. The Journal of neuroscience: the official journal of the Society for Neuroscience. 1992; 12:4565–4574. [PubMed: 1432110]

Reynolds BA, Weiss S. Generation of neurons and astrocytes from isolated cells of the adult mammalian central nervous system. Science. 1992; 255:1707–1710. [PubMed: 1553558]

Ridley AJ, Paterson HF, Johnston CL, Diekmann D, Hall A. The small GTP-binding protein rac regulates growth factor-induced membrane ruffling. Cell. 1992; 70:401–410. [PubMed: 1643658]

Roepstorff K, Grandal MV, Henriksen L, Knudsen SL, Lerdrup M, Grovdal L, Willumsen BM, van Deurs B. Differential effects of EGFR ligands on endocytic sorting of the receptor. Traffic. 2009; 10:1115–1127. [PubMed: 19531065]

Ruffjamison S, Chen K, Cohen S. Induction by Egf and Interferon-Gamma of Tyrosine-Phosphorylated DNA-Binding Proteins in Mouse-Liver Nuclei. Science. 1993a; 261:1733–1736. [PubMed: 8378774]

Ruffjamison S, Mcglade J, Pawson T, Chen K, Cohen S. Epidermal Growth-Factor Stimulates the Tyrosine Phosphorylation of Shc in the Mouse. Journal of Biological Chemistry. 1993b; 268:7610–7612. [PubMed: 7681824]

Ruffjamison S, Zhong Z, Wen ZL, Chen K, Darnell JE, Cohen S. Epidermal Growth-Factor and Lipopolysaccharide Activate Stat3 Transcription Factor in Mouse-Liver. Journal of Biological Chemistry. 1994; 269:21933–21935. [PubMed: 8071311]

Sato T, van Es JH, Snippert HJ, Stange DE, Vries RG, van den Born M, Barker N, Shroyer NF, van de Wetering M, Clevers H. Paneth cells constitute the niche for Lgr5 stem cells in intestinal crypts. Nature. 2011; 469:415-+. [PubMed: 21113151]

Schlessinger J. Receptor tyrosine kinases: legacy of the first two decades. Cold Spring Harbor perspectives in biology. 2014; 6

Schneider MR, Yarden Y. The EGFR-HER2 module: a stem cell approach to understanding a prime target and driver of solid tumors. Oncogene. 2016; 35:2949–2960. [PubMed: 26434585]

Shen Q, Wang Y, Kokovay E, Lin G, Chuang SM, Goderie SK, Roysam B, Temple S. Adult SVZ stem cells lie in a vascular niche: a quantitative analysis of niche cell-cell interactions. Cell stem cell. 2008; 3:289–300. [PubMed: 18786416]

Sibilia M, Wagner EF. Strain-dependent epithelial defects in mice lacking the EGF receptor. Science. 1995; 269:234–238. [PubMed: 7618085]

Singh B, Coffey RJ. Trafficking of epidermal growth factor receptor ligands in polarized epithelial cells. Annual review of physiology. 2014; 76:275–300.

Strunk KE, Amann V, Threadgill DW. Phenotypic variation resulting from a deficiency of epidermal growth factor receptor in mice is caused by extensive genetic heterogeneity that can be genetically and molecularly partitioned. Genetics. 2004; 167:1821–1832. [PubMed: 15342520]

Sun Y, Goderie SK, Temple S. Asymmetric distribution of EGFR receptor during mitosis generates diverse CNS progenitor cells. Neuron. 2005; 45:873–886. [PubMed: 15797549]

Tavazoie M, Van der Veken L, Silva-Vargas V, Louissaint M, Colonna L, Zaidi B, Garcia-Verdugo JM, Doetsch F. A specialized vascular niche for adult neural stem cells. Cell stem cell. 2008; 3:279–288. [PubMed: 18786415]

Threadgill DW, Dlugosz AA, Hansen LA, Tennenbaum T, Lichti U, Yee D, LaMantia C, Mourton T, Herrup K, Harris RC, et al. Targeted disruption of mouse EGF receptor: effect of genetic background on mutant phenotype. Science. 1995; 269:230–234. [PubMed: 7618084]

Wieduwilt MJ, Moasser MM. The epidermal growth factor receptor family: biology driving targeted therapeutics. Cellular and molecular life sciences: CMLS. 2008; 65:1566–1584. [PubMed: 18259690]

Wilson KJ, Gilmore JL, Foley J, Lemmon MA, Riese DJ 2nd. Functional selectivity of EGF family peptide growth factors: implications for cancer. Pharmacology & therapeutics. 2009; 122:1–8. [PubMed: 19135477]

Xia Y, Kao WW. The signaling pathways in tissue morphogenesis: a lesson from mice with eye-open at birth phenotype. Biochemical pharmacology. 2004; 68:997–1001. [PubMed: 15313393]

Zieske JD, Takahashi H, Hutcheon AE, Dalbone AC. Activation of epidermal growth factor receptor during corneal epithelial migration. Investigative ophthalmology & visual science. 2000; 41:1346–1355. [PubMed: 10798649]

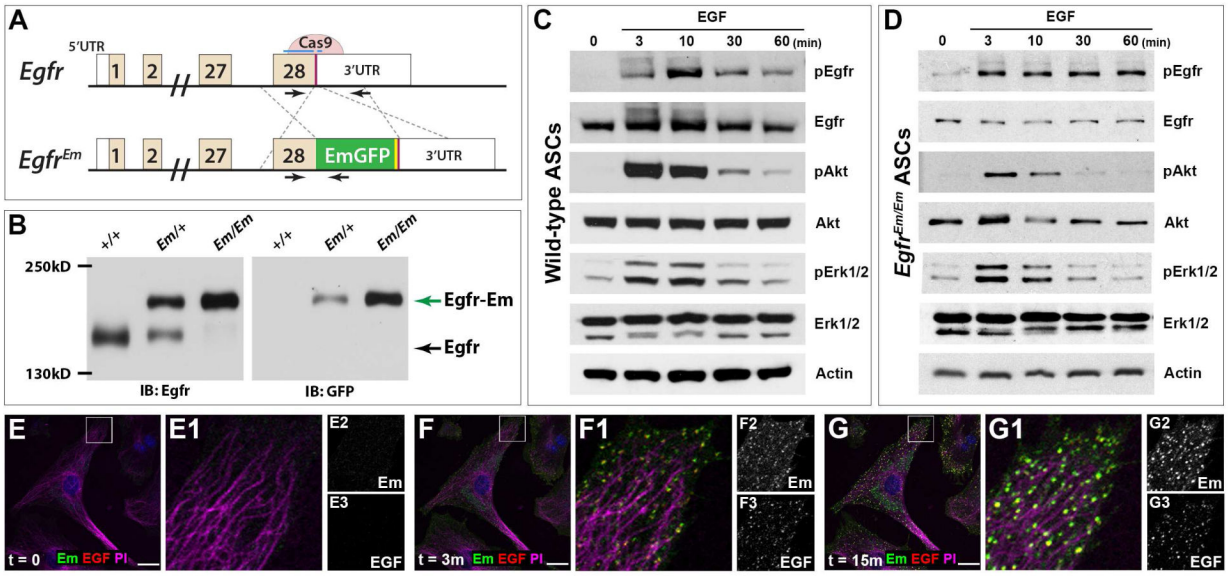

Figure 1. Generation, validation, and visualization of the *Egfr*^{Em} reporter mouse

(A) Targeting strategy via CRISPR/Cas9 genome editing to generate the *Egfr*^{Em} knock-in mouse reporter line. Fluorescent tag (EmGFP in green) followed by a V5 tag (yellow) was fused in frame and proximal to the stop codon (red bar) in exon 28 at the endogenous *Egfr* locus. UTR, untranslated region. Arrows denote primers for PCR genotyping. **(B)** Immunoblot analysis of adult mouse brain of various genotypes using anti-Egfr and anti-GFP antibodies. **(C, D)** EGF (50 ng/ml) was added to primary cultures of ASC of wild-type (C) and *Egfr*$^{Em/Em}$ mice (D) and signaling responses were monitored over time. **(EG)** Rhodamine-conjugated EGF (50 ng/ml) was added to serum-starved, ASC cultures from *Egfr*$^{Em/Em}$ mice. Rhodamine-EGF and Egfr-Em were monitored by time lapse microscopy. Right panels in E–G represent higher power images from insets of left panels of merge (E1, F1, G1) or single channels (E2,3; F2,3; G2,3). Em, Egfr-Em; Pl, phallodin. Scale bars, 25 μm.

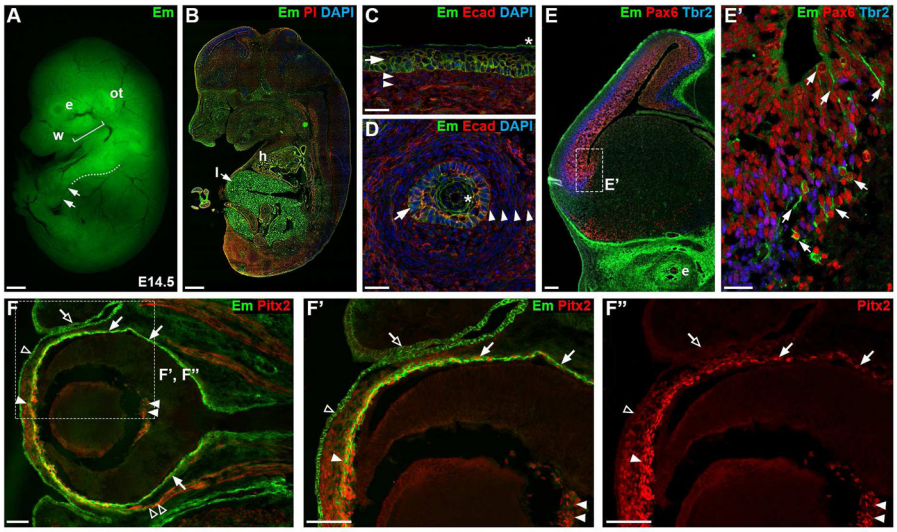

Figure 2. Egfr-Em expression in E14.5 embryo

(A) Wholemount E14.5 *Egfr*$^{Em/Em}$ embryo by direct fluorescence. E, eye; w, whisker follicles; ot, otic placodes. Arrows, interphalangeal zones of the forelimb. Scale bar, 400 μm. **(B)** A sagittal section of an E14.5 *Egfr*$^{Em/Em}$ embryo immunostained to visualize Egfr-Em (Em). L, liver; h, heart. Scale bar, 400 μm. (**C**) Egfr-Em was detected in the epidermis (arrow) but not the dermis (double arrowheads). Asterisk, unspecific staining at the keratinized layer of the skin. (**D**) Egfr-Em was found in the inner root sheath (arrow) and the center of the hair shaft (asterisk) but not in the outer root sheath (arrowheads) of the whisker follicles. Scale bars (C,D), 25 μm. (**E, E′**) In the SVZ, Egfr-Em was found in a subset of Pax6-expression radial glia progenitor cells (arrows in E′) but rarely found in the Tbr2^{+} intermediate progenitor cells. Scale bars, 100 μm in (E) and 25 μm in (E′). (**F–F″**) Egfr-Em co-localized with Pitx2 in periocular domains in the embryonic eye, including the extraocular mesenchyme (solid arrows), corneal mesenchyme (single solid arrowhead), hyaloid vasculature in the vitreous (double solid arrowheads), and extraocular muscles (double open arrowheads). Egfr-Em was also present in the palpebral and bulbar conjunctiva and in the eyelid epithelium (open arrow), and in the corneal epithelium (open arrowhead). Scale bars (F–F″), 100 μm.

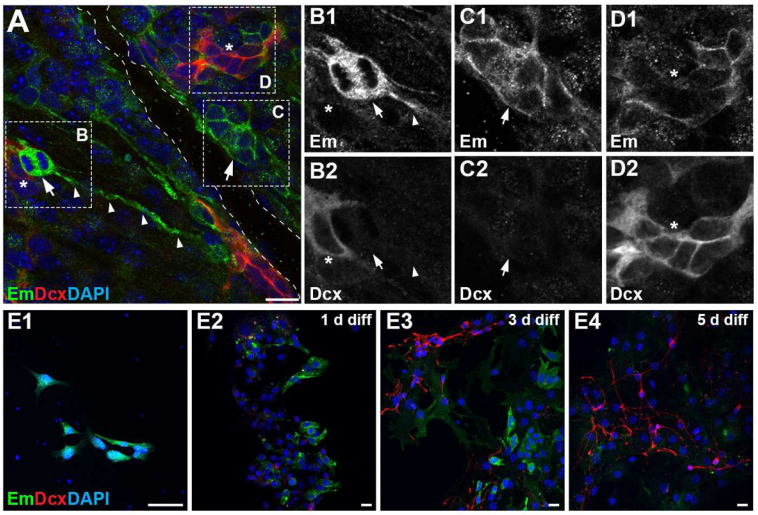

Figure 3. Egfr-Em^{+} cells are likely C cells and activated B1 neural progenitor cells

(**A–D**) Confocal images (*en face*) of a V-SVZ in *Egfr*^{Em} adult brain. (**A,B**) A putative aB1 cell that is Egfr-Em^{+}DCX^{-} (arrow in inset B, B1,2) is shown in the process of division adjacent to the ventricular surface and with a deeper basal process (white arrowheads) approaching a blood vessel (dotted outline). Asterisk in B, an Egfr-Em^{-}DCX^{+} A cell adjacent to the putative activated B1 cell. (**C,D**) A cluster of perivascular candidate C cells (Egfr-Em^{+}DCX^{-}; arrow in inset C, C1,2) and A cells (Egfr-Em^{-}DCX^{+}; asterisks in inset D, D1,2) are also detected. (**E**) Expression of Egfr-Em in V-SVZ neurospheres at various time points before and after growth factor withdrawal. When maintained in the presence of growth factors, a majority of cells express Egfr-Em (E1). As the neural progenitors differentiate after removal of EGF and bFGF, the number of Egfr-Em^{+} cells decreases as the number of DCX^{+} A cells (neuroblasts) increases (E2–4). Note the Egfr^{-} Em^{+} and DCX^{+} cells remain distinct populations throughout differentiation. Scale bars, 100 μm.

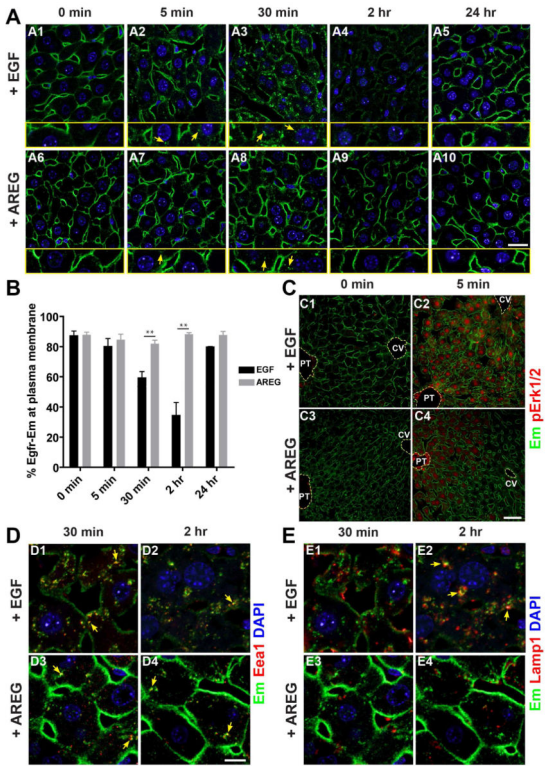

Figure 4. Egfr trafficking in hepatocytes following systemic administration of EGF or AREG

(A) Egfr-Em is mainly localized at the plasma membrane of hepatocytes at baseline (A1,6). Following an i.p. bolus of recombinant EGF, there is a progressive decrease in Egfr-Em at the plasma membrane from 5 minutes to 2 hours before it returns to baseline distribution at 24 hours (A2–5). This coincides with progressive increase in punctate cytosolic Egfr-Em at 5 and 30 minutes (A2,3) that is much reduced at 2 hours (A4) and largely absent at 24 hours (A5). In marked contrast, following an equimolar i.p. bolus of recombinant AREG, Egfr-Em remains largely at the plasma membrane throughout the 24-hour time course (A6–10), although some punctate cytosolic staining is seen at 5 and 30 minutes (A7,8). Arrows in the magnified images (yellow boxes), cytoplasmic Egfr-Em. Scale bar, 20 μm. **(B)** Proportion of Egfr-Em at the plasma membrane was calculated by normalizing its fluorescence intensity to that of the plasma membrane marker, Na^+/K^+ ATPase (**, $p < 0.01$). Data are presented as mean ± SEM. (**C**) Hepatocytes rarely show phosphorylated Erk1/2 before Egfr ligand treatment (C1, C3). Upon EGF treatment, Erk1/2 is phosphorylated and present in the nuclei and cytoplasm throughout the hepatocytes at 5 minutes (C2). In contrast, expression of pErk1/2 shows differential pattern in different regions, present near the portal tracts (PT) and absent near the central veins (CV) upon AREG treatment (C4). Scale bar, 50 μm. **(D, E)** Subcellular localization of Egfr-Em was analyzed using early endosomal marker, Eea1 (D), and lysosomal marker, Lamp1 (E). Most of the internalized Egfr-Em is in the endosomal compartment at 30 minutes (arrows in D1) and in the lysosomal compartment at two hours after EGF treatment (arrows in E2). In contrast, after AREG treatment, some internalized Egfr-Em is seen in the endosomal compartment (arrows in D3,4); however, rarely is it detected in the lysosomal compartment (E3,4). Scale bar, 10 μm.

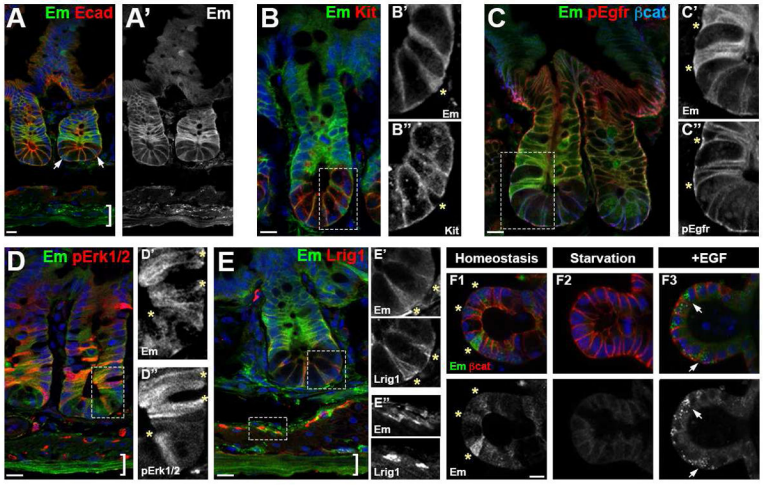

Figure 5. Distinct patterns of Egfr-Em expression in small intestine

(A) Egfr-Em was enriched in both the crypt versus villous compartment and in the outer longitudinal (bracket in A) versus inner circular muscle. Arrows, cytoplasmic Egfr-Em. Em, Egfr-Em; Ecad, E-cadherin. (**B**) Within the crypt compartment, staining was present in cells in the transit-amplifying zone and in crypt base columnar cells interspersed among c-Kit (Kit)-expressing Paneth cells. (B′, B″) Higher power single channel images of inset in (B). Asterisks, Egfr-Em^{+}c-Kit^{-} crypt base columnar cell. **(C)** Egfr-Em and pEgfr show similar expression pattern in crypt compartment. (C′, C″) higher power single channel images of inset in (C). Asterisks, cells with cytosolic Em and membranous pEgfr. **(D)** Egfr-Em and pErk1/2 show largely overlapping expression pattern in epithelial cells within the crypt compartment. Scattered pErk1/2 staining was observed in unspecified cells in lamina propria. (D′, D″) higher power single channel images of inset in (D). Asterisks, stem and progenitor cells with enriched Egfr-Em and pErk1/2. **(E)** Lrig1 co-express with Egfr-Em in the stem cells (E′) but not in the ICCs (E″). (E′,E″) higher power single channel images of top and bottom insets in (E) with asterisks showing co-expression of Em and Lrig1. **(F)** Scattered cells show cytoplasmic Egfr-Em when *Egfr*$^{Em/Em}$ colonoids were cultured in complete medium (asterisks in F1). Only weak membranous Egfr-Em fluorescence was detected 24 hours after withdrawal of serum and growth factors (F2). Largely cytoplasmic Egfr-Em fluorescence was observed 30 minutes following EGF stimulation (200ng/mL) (F3). Brackets in (A, D, E), outer longitudinal muscle. Scale bars, 10 μm.

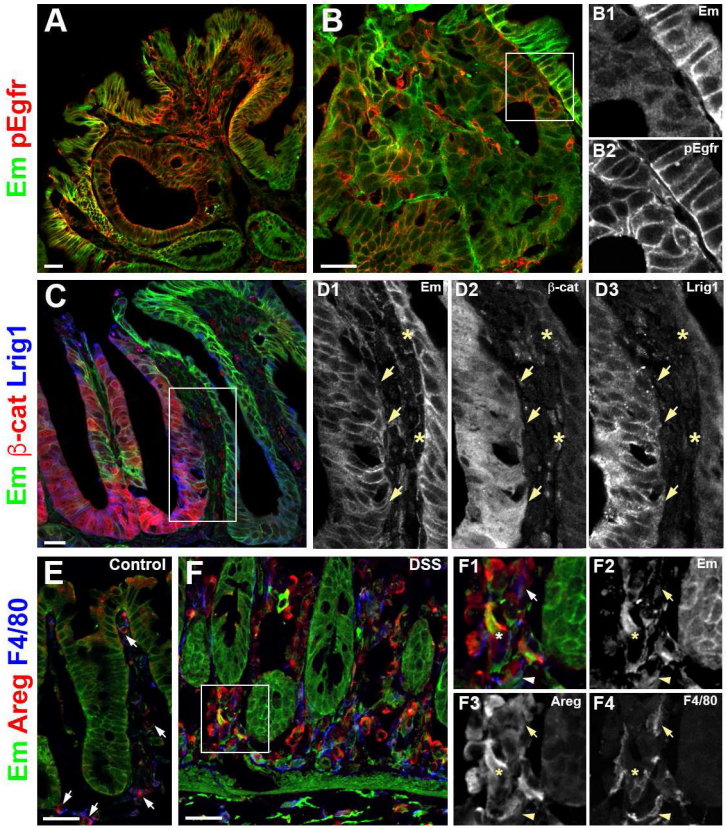

Figure 6. Egfr-Em expression under pathological conditions

(A, B) Immunodetection of Egfr-Em and pEgfr in the *Lrig1*$^{CreER/+}$;*Apc*$^{fl/+}$; *Egfr*$^{Em/+}$ intestinal adenomas. (B1, 2) Enlarged views of inset in (B) showed distinct expression pattern of Egfr-Em and pEgfr. (**C, D**) In the adenoma of *Lrig1*$^{CreER/+}$;*Apc*$^{fl/+}$; *Egfr*$^{Em/+}$, higher Egfr-Em expression was detected in the area that expressed lower β-catenin (D1–3, arrows). Lower Egfr-Em was often time associated with higher β-catenin and higher Lrig1 expression (arrows in D1–3). Higher Egfr-Em expression was found in Lrig1^{LO}β-catenin^{LO} cells (asterisks in D1–3). (**E–F**) Immunostaining of Egfr-Em, Areg, with F4/80 (E,F) in the control *Egfr*$^{Em/+}$ colon (E) and the *Egfr*$^{Em/+}$ colon after 7 days of DSS treatment (F). (F1–4) Arrows, Egfr-Em^{+}Areg^{+}F4/80^{+}; arrowheads, Egfr-Em^{+}Areg^{-}F4/80^{+}; asterisks, Egfr-Em^{+}Areg^{+}F4/80^{-}.